NANO LETTERS

pubs.acs.org/NanoLett

Deterministic Coupling of a Single Nitrogen Vacancy Center to a Photonic Crystal Cavity

Dirk Englund,*,†,⊥ Brendan Shields,†,⊥ Kelley Rivoire,§ Fariba Hatami,∥ Jelena Vučković,§ Hongkun Park,*,‡ and Mikhail D. Lukin*,†

†Department of Physics and ‡Department of Chemistry and Chemical Biology, Harvard University, Cambridge Massachusetts 02138, §Department of Electrical Engineering, Stanford University, Stanford California 94305, and ∥Department of Physics, Humboldt-Universität zu Berlin, Newtonstrasse 15, 12489 Berlin

ABSTRACT We describe and experimentally demonstrate a technique for deterministic, large coupling between a photonic crystal (PC) nanocavity and single photon emitters. The technique is based on in situ scanning of a PC cavity over a sample and allows the precise positioning of the cavity over a desired emitter with nanoscale resolution. The power of the technique is demonstrated by coupling the PC nanocavity to a single nitrogen vacancy (NV) center in diamond, an emitter system that provides optically accessible electron and nuclear spin qubits.

KEYWORDS Nitrogen-vacancy (NV) center, diamond, qubit, spin dynamics, cavity QED, photonic crystal

Optical resonators enable large amplification of small optical signals, resulting in a range of spectroscopic and sensing applications, and have allowed for detection of single atoms,[6] molecules,[7] and quantum dots.[3,8] In addition, they enable a controllable coupling between optical emitters and the cavity vacuum field that is critical for efficient light sources[2,4,5] and for the realization of memory nodes in quantum networks[9] and quantum repeaters.[10] This coupling strength scales with the cavity mode volume V_m as $1/(V_m)^{1/2}$, and consequently, nanoscale photonic crystal (PC) cavities have been explored extensively in solid-state cavity QED applications. While much progress has been achieved in coupling quantum dots to PC cavities made from the host material,[1,3,11] extending these techniques to fully deterministic coupling and to other material systems has been difficult. Specifically, there has been much recent interest in coupling PC resonators to NV centers,[12−15] a promising single photon emitter with excellent electronic and nuclear spin memory,[16−18] though experimental demonstrations have remained a challenge.

In this letter, we demonstrate a technique for deterministic positioning of micrometer-scale PC slabs that support high quality factor (Q) cavity modes with nanometer-scale features. When such a cavity is scanned over the sample, it can be used for deterministic coupling to optically active systems with subwavelength resolution via the evanescent field. By appropriate design of PC cavities and waveguides, these systems combine subwavelength resolution, high throughput, and cavity-enhanced sensitivity. In particular, they can be deterministically interfaced with isolated optical emitters.

In our experiments, the PC consists of a triangular lattice of air holes in a gallium phosphide (GaP) membrane, creating an optical bandgap that confines light in the slab to a cavity region. The bandgap along the ΓJ crystal direction is shown in the dispersion diagram in Figure 1a. Confinement in the vertical direction occurs through total internal reflection (TIR) for modes with frequencies below the air light-line indicated in Figure 1a. A row of missing holes supports band modes that form bound cavity states when terminated on two sides. We employ a three-hole defect cavity[19] whose geometry is optimized for use on a poly(methyl methacrylate) (PMMA) substrate with a refractive index of $n_s \sim 1.5$ (see Supporting Information). The TIR-confined region in k-space is smaller on top of the PMMA, as sketched in Figure 1a, but simulations indicate that the Q value can still be above 13×10^3. The cavity has a mode volume $V_m = 0.74(\lambda/n_{GaP})^3$, where $n_{GaP} = 3.4$ is the refractive index of GaP at $\lambda = 670$ nm. The fundamental mode of the PC cavity is depicted by its energy density in Figure 1c. The cross section in Figure 1b shows the evanescent tail of the mode that couples to emitters.

We fabricate GaP PC nanocavities by a combination of electron beam lithography and dry etching[20] of a 108 nm membrane of GaP on top of a 940 nm-thick sacrificial layer of a $Al_{0.85}Ga_{0.15}P$. A wet etch removes the sacrificial layer, leaving free-standing photonic crystal membranes. The scanning electron micrograph (SEM) of a resulting PC nanocavity is shown in Figure 1d. Reflectivity measurements of freestanding cavities indicate that quality factors of these cavities can exceed 6×10^3, the maximum value that can be measured with the resolution of our spectrometer (Figure 1f). However, in the remainder of this paper, we will study

* To whom correspondence should be addressed. E-mail: (D.E.) englund@columbia.edu; (H.P.) Hongkun_Park@harvard.edu; (M.D.L) lukin@physics.harvard.edu.

⊥ These authors contributed equally to this paper.

Received for review: 05/10/2010
Published on Web: 09/08/2010

DOI: 10.1021/nl101662v | *Nano Lett.* **2010,** *10,* 3922–3926

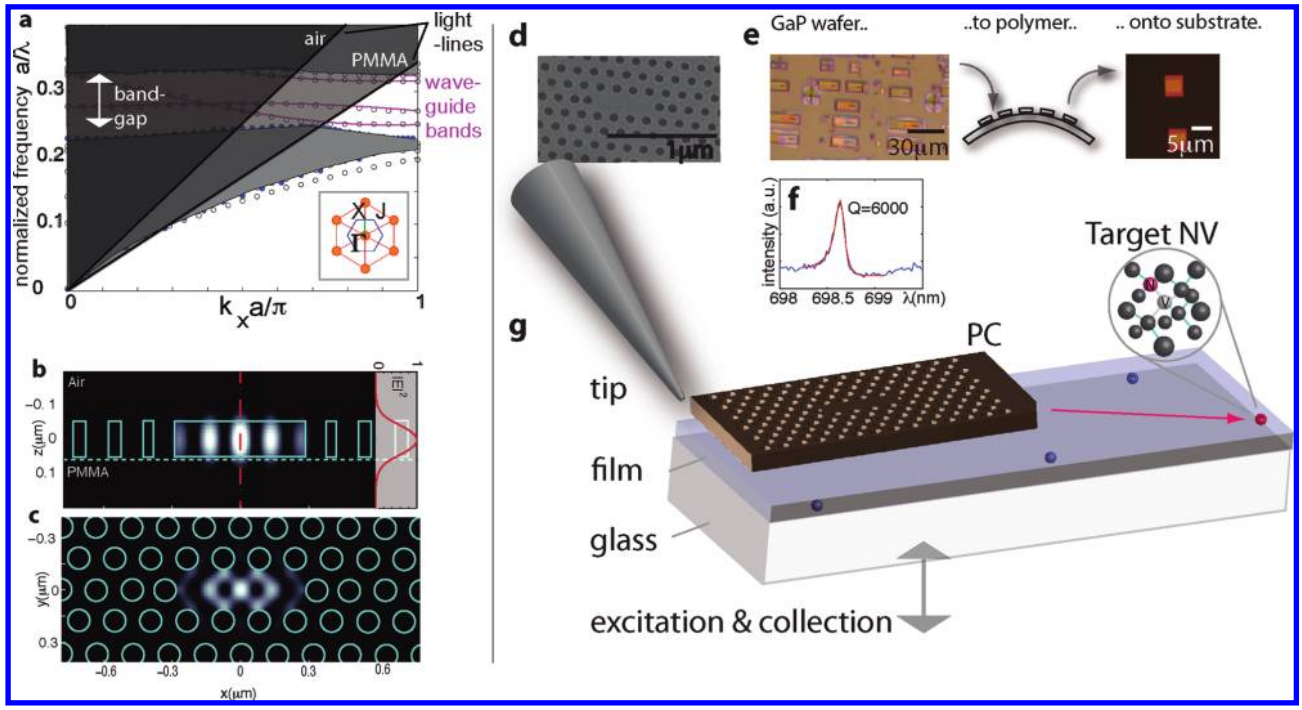

FIGURE 1. (a) Dispersion for the photonic crystal slab in air, along the waveguide direction k_x; the inset shows the reciprocal lattice (orange) and the first Brillouin zone (blue). The lattice has a periodicity of $a = 176$ nm, hole radius of ~53 nm, and slab height of ~110 nm. (b) Energy density for fundamental mode in cross-section and (c) in plane. (d) SEM. (e) The photonic crystals are transferred from the GaP chip onto a substrate via a polymer stamp. (f) Broad-band reflectivity measurement of a cavity resonance with $Q \approx 6 \times 10^3$. (g) The PC slab is positioned relative to a target nanocrystal in the polymer film.

cavities with typical Q values below 1000, since these were more reliably fabricated in large numbers, permitting systematic studies. To transfer cavities, we press the GaP chip against a flexible polymer layer of polydimethylsiloxane (PDMS), which separates the PC membranes from the chip while preserving their arrangement. The adhesion between the membranes and the PDMS is weak enough so that the GaP structures can be stamped onto the sample that is to be imaged, as shown in Figure 1e. In our demonstration, the sample consists of ~30 nm diamond nanocrystals that are dispersed on a glass slide covered by a 100 nm thick layer of PMMA for which the transfer process succeeds with ~80% probability for each membrane. The sample is mounted in a scanning confocal microscope with an oil immersion lens. A tungsten tip with radius <0.5 μm is used to scan and position a PC nanocavity with nanometer resolution (Figure 1g).

Figure 2a shows a room-temperature photoluminescence (PL) image of a typical sample (red signal) obtained by scanning a green excitation laser across the surface with galvanometric mirrors. The PL spots in the image correspond to single or clusters of NV centers in diamond nanocrystals. The PC nanocavity can be located with the excitation laser reflection (green in Figure 2a) as well as weak fluorescence originating from impurities in GaP and PMMA (green curve in Figure 2c). The PC fluorescence clearly shows two resonances at $\lambda_1 = 667.3$ nm and $\lambda_2 = 643.0$ with quality factors $Q_1 = 550$ and $Q_2 = 610$. These quality factors are rather low because of variabilities in the fabrication; we saw no degradation due to the transfer onto the PMMA substrate. By collecting the spectrum at different points within the cavity (see Supporting Information), we can identify peak 1 as the fundamental mode depicted in Figure 1c and peak 2 as two nearly degenerate, oppositely polarized higher-order modes of the cavity.

We achieve deterministic coupling between the NV and the nanocavity by first selecting a "target" NV (indicated in Figure 2a). This center exhibits a broad spectrum I_0 (Figure 2c), which is characteristic of NV centers and results from a broad phonon sideband extending from ~640 to 800 nm. Importantly, the emission exhibits a strongly antibunched autocorrelation (inset), indicating that it results from a single emitter. To couple this emitter to the cavity, we position the PC membrane over the target NV using the tungsten tip. As shown in Figure 2d, the PL spectrum I_c changes dramatically and shows strong peaks on resonance with the cavity modes. The intensities of these peaks are far higher than the cavity background, I_{cb}. Moreover, the autocorrelation of the coupled NV-cavity system is again strongly antibunched (Figure 2d), indicating that the observed fluorescence is due to the NV center; this is supported by photon correlation measurements on the filtered cavity emission, given in the Supporting Information. We also verified the electronic triplet state of the coupled NV by measurements of the electron spin resonance (ESR) and Rabi oscillation, also given in the Supporting Information.

DOI: 10.1021/nl101662v | *Nano Lett.* **2010,** *10,* 3922–3926

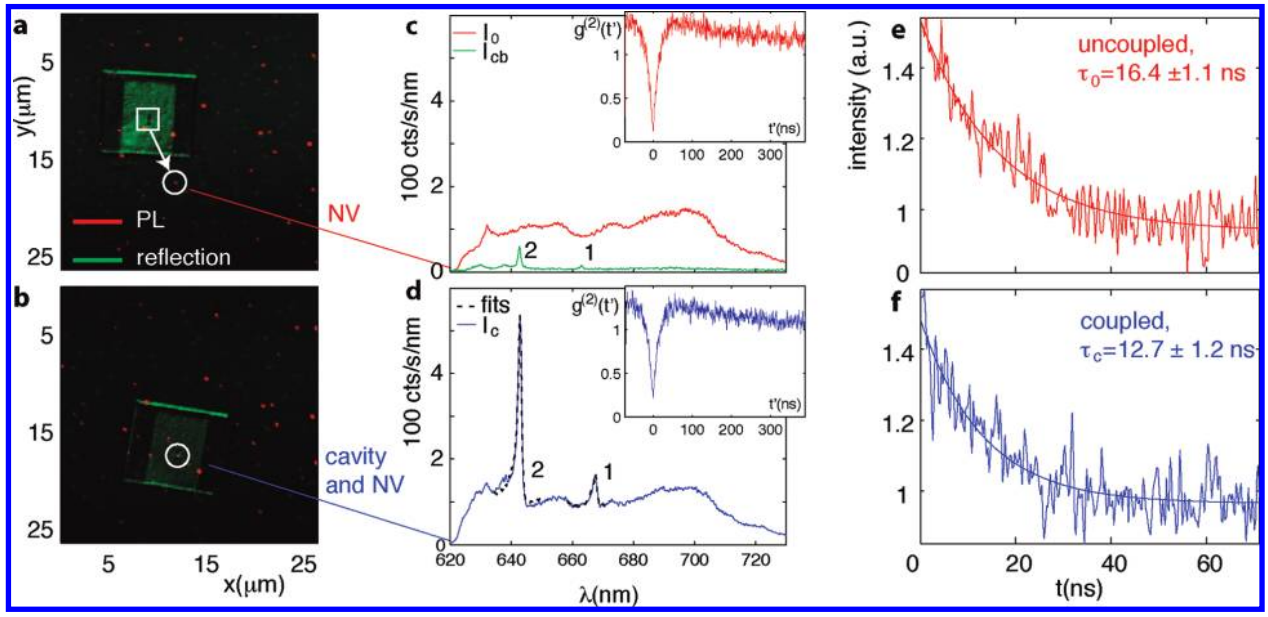

FIGURE 2. The photonic crystal is moved from an initial uncoupled position (a) into alignment with the target NV center (b). The pump laser reflectivity is shown in green and the photoluminescence in red; pump laser power is 500 μW, focused to ~0.2 μm. (c) PL spectrum of the uncoupled NV (I_0) and uncoupled cavity background (I_{cb}). A photon correlation measurement shows that the NV emission is strongly antibunched (inset); this feature is surrounded by photon bunching due to shelving in a metastable state of the NV emitter.[21] (d) PL spectrum I_c of the coupled NV-cavity system, again strongly antibunched (inset). A fit to theory (eq 1) gives the SE rate into the cavity normalized by the background emission rate, $f^c(\lambda_2) = 5.3, f^c(\lambda_1) = 0.7$. (e) Time-resolved emission for the uncoupled NV, far removed from the PC membrane, and (f) the coupled NV. The 6 ps excitation pulse was generated by a frequency-doubled 1064 nm laser at 20 MHz repetition.

The SE rate of an NV center is also modified by the presence of the PC slab. Specifically, Figure 2e,f shows that the lifetimes of the uncoupled and coupled NV centers are $\tau_{0,c} = 16.4 \pm 1.1, 12.7 \pm 1.5$ ns, respectively. The lifetime reduction is attributed primarily to the increased refractive index surrounding the NV. The PL spectra on and off the PC coupled with lifetime measurements allow the determination of the spectrally resolved SE rate enhancement, $F(\lambda)$, of the coupled emitter via the relation $F(\lambda) = I_c(\lambda)\tau_0/I_0(\lambda)\tau_c$ (see Supporting Information); the analysis of the data in Figure 2 yields $F(\lambda_1) = 2.2$ and $F(\lambda_2) \sim 7.0$ (the full curve $F(\lambda)$ is plotted in the Supporting Information).

We next demonstrate the spatial resolution of our method. By monitoring the fluorescence spectrum while scanning the cavity over the NV, we can map out the near-field emitter-cavity coupling. This is demonstrated in Figure 3a−e, where we scan the cavity along its longitudinal (x-axis) over the sample in 3.4 nm steps. Figure 3f presents a series of PL spectra acquired as the cavity moves over the emitter and reveals an intensity oscillation with a period corresponding to one PC lattice spacing, $a \sim 180$ nm. This oscillation corresponds to the spatially dependent SE modification, which is directly proportional to the cavity's electric field intensity.

To analyze our observations, we note that the fluorescence of the coupled NV-cavity system is given by the emission directly from the NV, the emission through the cavity, and interference between the two

$$S_d(\omega, \vec{r}) = C_{NV} + C_{cav} f^c(\vec{r}) \left| L(\omega) \right|^2 + 2C_{int} R[e^{i\Delta\phi} \sqrt{f^c(\vec{r})} L(\omega)] \quad (1)$$

where C_{NV}, C_{cav}, and C_{int} determine the relative contributions of the NV, the cavity, and their interference, respectively, which depend on the collection geometry and coupling to the collection fiber. $L(\omega) = 1/(1 + i(\omega - \omega_c)/\kappa)$ gives the Lorentzian line shape of the cavity resonance at ω_c with line width $\kappa = \omega_c/2Q$, and $\Delta\phi$ accounts for the phase difference at the collection point between the direct NV emission and the emission through the cavity. The factor $f^c(\omega, \vec{r})$ is the SE rate enhancement of transitions in the phonon sideband of the NV with respect to the background emission rate into noncavity modes.

The coefficients C_{NV}, C_{cav}, and C_{int} can be estimated from our experimental data as follows. Because of the high numerical aperture of our objective, nearly half of the emission from the cavity and the NV is collected; this observation suggests $C_{NV} \sim C_{cav}$. When the signal is collected through a single-mode fiber, the interference term represented by C_{int} becomes important and results in Fano-like features in the spectrum (see Supporting Information).[22] However, we find that the interference term vanishes when a multimode fiber is used, and we can set $C_{int} = 0$. A fit of eq 1 to the spectrum in Figure 2d then yields $f^c(\lambda = 643$ nm, $\vec{r}) = 5.3$, $f^c(667$ nm, $\vec{r}) = 0.7$.

DOI: 10.1021/nl101662v | *Nano Lett.* **2010,** *10,* 3922--3926

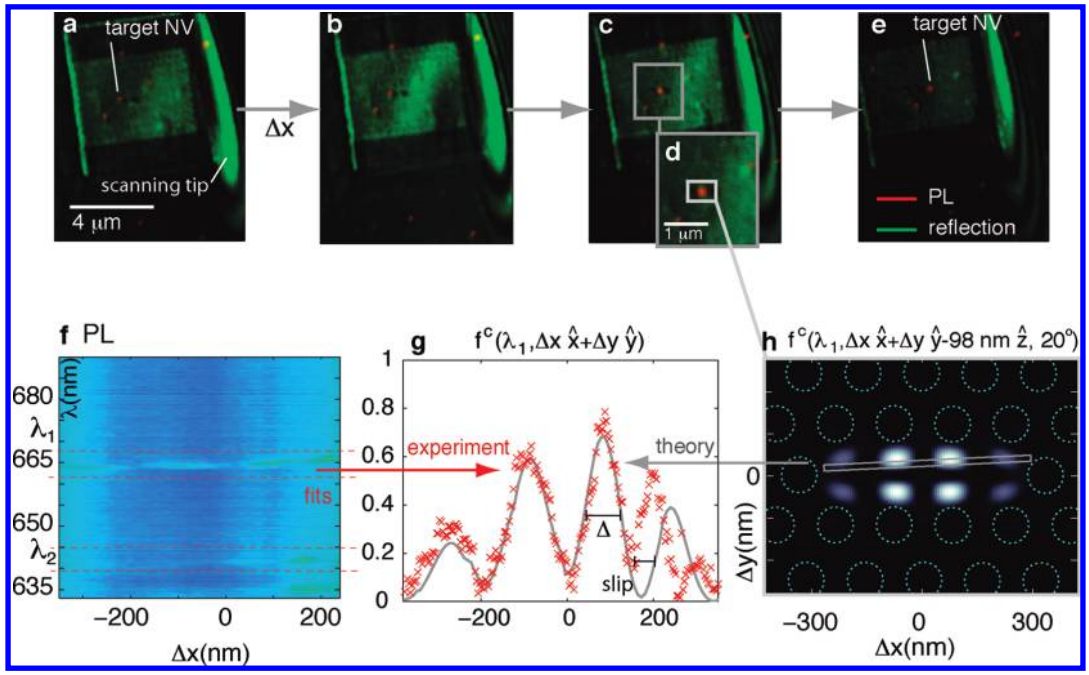

FIGURE 3. Scanning of the PC nanocavity probe in small steps, shown in snap-shots (a−e). (f) Photoluminescence scans for $\langle \Delta x \rangle = 3.4$ nm average step sizes. (g) Fitted cavity SE rate enhancements $f^c(\lambda_1, \vec{r})$ for mode 1 showing a fwhm resolution of $\Delta \sim 80$ nm. (h) Expected SE enhancement factor $f^c(\lambda_1, \vec{r})$ and the estimated trajectory of the NV at $\Delta z = 98 \pm 5$ nm, $\Delta y = 70 \pm 5$ nm, and $\vec{\mu}$ in the plane at 20° to the x-axis. The indicated track matches the observed SE enhancement in (g).

Since the signal in Figure 3f is proportional to $S_d(\omega, \vec{r})$, we can now use eq 1 to compare the measured cavity signal to theory. Figure 3g plots the fitted values of $f^c(\omega_1, \vec{r})$ for the fundamental cavity mode frequency $\omega_1 = 2\pi c/\lambda_1$, as shown in the red crosses. By comparing the experimental $f^c(\omega_1, \vec{r})$ values to predictions for the cavity mode, we find a match between experiment and theory for an NV dipole μ that is $z = 98 \pm 5$ nm from the PC surface, as expected from the PMMA thickness, and at an angle of 20° to the x-axis, obtained from the best fit to the data. For these conditions, the predicted value of SE rate modification corresponds to the track graphed in Figure 3h, which is in good agreement with experimental observations. A small discrepancy in the fit at $\Delta x \sim 190$ nm results primarily from positional slip of the PC cavity that can build up during the scan, a problem which could be improved by rigidly attaching the membrane to a stiffer scanning tip.

The high spatial resolution and frequency-selective modification of spontaneous emission opens new possibilities for efficient interfacing of promising solid state qubits via optical fields. For instance, while the NV center is a promising system for quantum information processing, only the emission occurring into the zero phonon line (ZPL) is suitable for coherent optical manipulation. The frequency-selective emission enhancement demonstrated here potentially allows us to direct most of the emission of the selected NV centers into the ZPL. Furthermore, the hybrid approach is compatible with narrow line width NV emitters in bulk diamond at low temperature. This opens the door for applications ranging from quantum repeaters to single photon nonlinear optics. Moreover, although we have focused here on NV centers, our scanning technique provides a "cavity QED interface" that can be of use to a broad range of solid state qubits.

Furthermore, the PC scanning technique can serve as a new imaging approach with subwavelength resolution and high throughput, which we term a scanning cavity microscope (SCM). Unlike other near-field probes that compromise the signal intensity to achieve high spatial resolution, SCM enables large count rates; in the demonstration shown here, we record up to $\sim 1 \times 10^6$ photons/s from a single NV, exceeding the collection with far field optics. This can be further improved by efficiently out-coupling through cavity-coupled waveguides. In addition, the spatial resolution of the SCM is determined by the feature size of the confined field, which is $\Delta \sim 80$ nm for this cavity. This in-plane resolution may be improved substantially using cavity modes with small feature sizes, as in slot-waveguide cavities.[23] These qualities make the SCM a promising tool for label-free single molecule studies[7,24] or high-resolution studies of local index variations in thin films.[25,26] Beyond high resolution and throughput, the SCM adds the capability to modify the spontaneous emission rate to near-field microscopy. This opens new possibilities for direct investigations of decay channels of optical emitters, such as light-emitting diodes or fluorophores; for instance, by monitoring the emission intensity while effecting a known change in the radiative emission rate, the relative nonradiative recombation rate may be inferred, allowing a direct estimate of the radiative quantum efficiency of the material.

DOI: 10.1021/nl101662v | *Nano Lett.* **2010,** *10,* 3922--3926

Supporting Information Available. Wavelength-resolved excited state recombination rates, photon correlation measurements, characterization of cavity modes, single mode fiber spectra, filtered cavity emission photon statistics, electron spin resonance and Rabi oscillations, spontaneous emission modification, imaging of general samples, and additional references. This material is available free of charge via the Internet at http://pubs.acs.org.

REFERENCES AND NOTES

(1) Yoshie, T.; Scherer, A.; Hendrickson, J.; Khitrova, G.; Gibbs, H. M.; Rupper, G.; Ell, C.; Shchekin, O. B.; Deppe, D. G. *Nature* **2004**, *432*, 200–203.

(2) Strauf, S.; Stoltz, N. G.; Rakher, M. T.; Coldren, L. A.; Petroff, P. M.; Bouwmeester, D. *Nat. Photonics* **2007**, *1*, 704–708.

(3) Englund, D.; Faraon, A.; Fushman, I.; Stoltz, N.; Petroff, P.; Vučković, J. *Nature* **2007**, *450*, 857–61.

(4) Fujita, M.; Takahashi, S.; Tanaka, Y.; Asano, T.; Noda, S. *Science* **2005**, *308*, 1296–1298.

(5) Englund, D.; Fattal, D.; Waks, E.; Solomon, G.; Zhang, B.; Nakaoka, T.; Arakawa, Y.; Yamamoto, Y.; Vuckovic, J. *Phys. Rev. Lett.* **2005**, *95*, No. 013904.

(6) Hood, C. J.; Lynn, T. W.; Doherty, A. C.; Parkins, A. S.; Kimble, H. J. *Science* **2000**, *287*, 1447–1453.

(7) Armani, A. M.; Kulkarni, R. P.; Fraser, S. E.; Flagan, R. C.; Vahala, K. J. *Science* **2007**, *317*, 783–787.

(8) Srinivasan, K.; Painter, O. *Nature* **2007**, *450*, 862–865.

(9) Cirac, J. I.; Zoller, P.; Kimble, H. J.; Mabuchi, H. *Phys. Rev. Lett.* **1997**, *78*, 3221–24.

(10) Briegel, H.-J.; Dür, W.; Cirac, J. I.; Zoller, P. *Phys. Rev. Lett.* **1998**, *81*, 5932–5935.

(11) Hennessy, K.; Badolato, A.; Winger, M.; Gerace, D.; Atature, M.; Gulde, S.; Falt, S.; Hu, E. L.; Imamoglu, A. *Nature* **2007**, *445*, 896–899.

(12) Barth, M.; Nüsse, N.; Löchel, B.; Benson, O. *Opt. Lett.* **2009**, *34*, 1108–1110.

(13) Barclay, P. E.; Fu, K.-M.; Santori, C.; Beausoleil, R. G. *Opt. Express* **2009**, *17*, 9588–9601.

(14) Bayn, I.; Salzman, J. *Opt. Express* **2008**, *16*, 4972–4980.

(15) Kreuzer, C.; Riedrich-Möller, J.; Neu, E.; Becher, C. *Opt. Express* **2008**, *16*, 1632–1644.

(16) Neumann, P.; Mizuochi, N.; Rempp, F.; Hemmer, P.; Watanabe, H.; Yamasaki, S.; Jacques, V.; Gaebel, T.; Jelezko, F.; Wrachtrup, J. *Science* **2008**, *320*, 1326–1329.

(17) Jiang, L.; Hodges, J. S.; Maze, J. R.; Maurer, P.; Taylor, J. M.; Cory, D. G.; Hemmer, P. R.; Walsworth, R. L.; Yacoby, A.; Zibrov, A. S.; Lukin, M. D. *Science* **2009**, *326*, 267–272.

(18) Fuchs, G. D.; Dobrovitski, V. V.; Toyli, D. M.; Heremans, F. J.; Awschalom, D. D. *Science* **2009**, 1181193.

(19) Akahane, Y.; Asano, T.; Song, B.-S.; Noda, S. *Nature* **2003**, *425*, 944–947.

(20) Rivoire, K.; Faraon, A.; Vuckovic, J. *Appl. Phys. Lett.* **2008**, *93*, No. 063103.

(21) Nizovtsev, A. P.; Kilin, S. Y.; Tietz, C.; Jelezko, F.; Wrachtrup, J. *Phys. B* **2001**, *308*−*310*, 608–611.

(22) Barclay, P. E.; Santori, C.; Fu, K.-M.; Beausoleil, R. G.; Painter, O. *Opt. Express* **2009**, *17*, 8081–8097.

(23) Robinson, J. T.; Manolatou, C.; Chen, L.; Lipson, M. *Phys. Rev. Lett.* **2005**, *95*, 143901.

(24) Moerner, W. E. *J. Phys. Chem. B* **2002**, *106*, 910–927.

(25) Pulker, H. K. *Appl. Opt.* **1979**, *18*, 1969–1977.

(26) Diziain, S.; Merolla, J.-M.; Spajer, M.; Benvenuti, G.; Dabirian, A.; Kuzminykh, Y.; Hoffmann, P.; Bernal, M.-P. *Rev. Sci. Instrum.* **2009**, *80*, No. 093706.

DOI: 10.1021/nl101662v | *Nano Lett.* **2010,** *10,* 3922–-3926